

Development of an early warning method incorporating pre-supernova neutrino light curves

K.SAITO,¹ M.EIZUKA,¹ Z.HU,^{2,3} K.ICHIMURA,¹ M.IKEDA,^{4,5} K.ISHIDOSHIRO,¹ N.KAWADA,¹ L.N.MACHADO,⁶ LL.MARTI,⁵ K.MIKAMI,¹ K.TACHIBANA,¹ AND R.A.WENDELL^{2,5}

¹*Research Center for Neutrino Science, Tohoku University, Sendai 980-8578, Japan*

²*Department of Physics, Kyoto University, Kyoto, Kyoto 606-8502, Japan*

³*Ecole Polytechnique, IN2P3-CNRS, Laboratoire Leprince-Ringuet, F-91120 Palaiseau, France*

⁴*Kamioka Observatory, Institute for Cosmic Ray Research, University of Tokyo, Kamioka, Gifu 506-1205, Japan*

⁵*Kavli Institute for the Physics and Mathematics of the Universe (WPI), The University of Tokyo Institutes for Advanced Study, University of Tokyo, Kashiwa, Chiba 277-8583, Japan*

⁶*School of Physics and Astronomy, University of Glasgow, Glasgow, Scotland, G12 8QQ, United Kingdom*

ABSTRACT

Massive stars ($M > 8M_{\odot}$) emit neutrinos known as pre-supernova (pre-SN) neutrinos through thermal and nuclear interactions for cooling the stellar core during the final stage of stellar evolution. Real-time monitoring of their pre-SN neutrino interaction rate offers a crucial opportunity to issue an early warning to a core-collapse supernova. Some neutrino detectors, including KamLAND and Super-Kamiokande already operate pre-SN alarm systems based on a statistically significant excess of the observed event rate over the expected background. To improve alarm sensitivity, we propose an alarm method which incorporates the time evolution of the observed pre-SN neutrino event rate. The method uses a log likelihood ratio test that references multiple theoretical stellar-evolution models and treats the core collapse time as a nuisance parameter to be profiled over. The performance of the proposed method was evaluated using simulated data for the KamLAND, Super-Kamiokande with dissolved Gadolinium (SK-Gd) and their combined analysis. The results demonstrate a significant improvement in the warning time compared to the conventional rate-only method, while maintaining the same false alarm rate.

1. INTRODUCTION

Core-collapse supernovae (CCSNe), in contrast to thermonuclear Type-Ia events, release a huge amount of energy in the form of neutrinos, gravitational waves and electromagnetic waves. The neutrino burst from a CCSN directly probes the stellar interior since neutrinos interact only via the weak force, whereas photons remain trapped in the envelope until much later. In 1987, Kamiokande-II (K. Hirata et al. (1987)), IMB (R. M. Bionta et al. (1987)) and Baksan (E. N. Alekseev et al. (1987)) achieved the first detection of the neutrino burst from SN1987A in the Large Magellanic Cloud, at a distance of ~ 50 kpc (G. Pietrzyński et al. (2019)). The time and energy distributions of the 24 events observed by the three detectors provided a standard picture of the explosion mechanism (G. Pagliaroli et al. (2009)). Current and future neutrino detectors are expected to yield more detailed understanding of the explosion mechanism from the next galactic CCSN (K. Scholberg (2012)).

A massive star with initial mass $\geq 8M_{\odot}$ at the Zero Age Main Sequence (ZAMS) emits neutrinos of all flavors during the late stages of stellar evolution. These “pre-supernova” (pre-SN) neutrinos are produced by thermal and nuclear processes in the stellar core. Their detections could provide an understanding of late-stage stellar evolution and the neutrino mass ordering (C. Kato et al. (2020)). Since these neutrinos are emitted before the core collapse, they can be used as an early warning to CCSNe.

In the sub-MeV to few-MeV energy range, relevant for pre-SN neutrino detection, the neutrino interactions are predominantly coherent neutrino-nucleus scattering, electron scattering and inverse beta decay. Inverse beta decay (IBD, $\bar{\nu}_e + p \rightarrow e^+ + n$) which has an energy threshold of 1.806 MeV, allows pre-SN electron antineutrinos to be observed by some large-volume neutrino detectors including KamLAND (A. Suzuki (2014)), Super-Kamiokande (Y. Fukuda et al. (2003)) loaded with gadolinium (SK-Gd, L. N. Machado et al. (2022)), JUNO (A. Abusleme et al. (2024)) and SNO+ (V. Albanese et al. (2021)), which have sufficient sensitivity to few-MeV signals. Furthermore, upcoming detectors such as DUNE (B. Abi et al. (2021)), Hyper-Kamiokande (K. Abe et al. (2018)) and 100 ton-

scale dark matter detectors (N. Raj et al. (2020)) are expected to be sensitive to pre-SN neutrinos. The SuperNova Early Warning System (SNEWS 2.0), an upgraded global network of neutrino observatories, aims to coordinate and disseminate pre-SN and supernova alerts (P. Antonioli et al. (2004), S. Al Kharusi et al. (2021)).

KamLAND (K. Asakura et al. (2016)) and Super-Kamiokande (L. N. Machado et al. (2022)) deployed pre-SN early-warning systems in 2015 and 2021, respectively. Furthermore, a combined pre-SN alarm system was launched in 2023 (S. Abe et al. (2024)).⁷ These systems issue an alarm with the statistical significance of a rate excess over the expected background. A. Sheshukov et al. (2021) proposed an approach that incorporates time evolution of neutrino luminosity, and demonstrated improved sensitivity relative to rate-only approach. However, the previous study evaluated alarm sensitivity for cases where the core collapse time was given. Therefore our work presents a crucial update: we conduct a statistical test that includes the estimated core collapse time. This paper presents an alarm method using a rate and time based likelihood function with estimation of core collapse time. Also, we evaluate the alarm significance injected from various pre-SN neutrino light curve models and mass orderings.

The structure of this paper is as follows. Section 2 introduces the pre-SN neutrino models used in this study. Sections 3 and 4 describe the configurations and background conditions of KamLAND and Super-Kamiokande. Section 5 reviews the conventional alarm methods. In Section 6, we present our light-curve-based approach. The performance results are reported in Section 7 and discussed in Section 8. Finally, Section 9 summarizes the conclusions.

2. PRE-SUPERNOVA NEUTRINO LIGHT CURVE MODEL

The evolution of massive stars proceeds through successive nuclear burning stages of hydrogen, helium, carbon, neon and silicon. After the carbon-burning stage, neutrinos dominate the energy transport from the core, where the temperatures reach over $\sim 10^8$ K. While all flavors of neutrino and antineutrino pairs are produced thermally via $e^- + e^+ \rightarrow \nu + \bar{\nu}$, weak nuclear interactions such as beta decays and electron/positron captures become dominant after the Si-burning stage.

For this analysis, the expected pre-SN neutrino rate in each detector is evaluated using established pre-SN neutrino light curve models including A. Odrzywolek et al. (2004), A. Odrzywolek & A. Heger (2010), C. Kato et al. (2015), T. Yoshida et al. (2016), C. Kato et al. (2017) and K. M. Patton et al. (2017). These models are based on numerical one dimensional hydrodynamical simulations of the late stages of stellar evolution and have advanced our understanding of the pre-SN neutrino flux and spectrum.

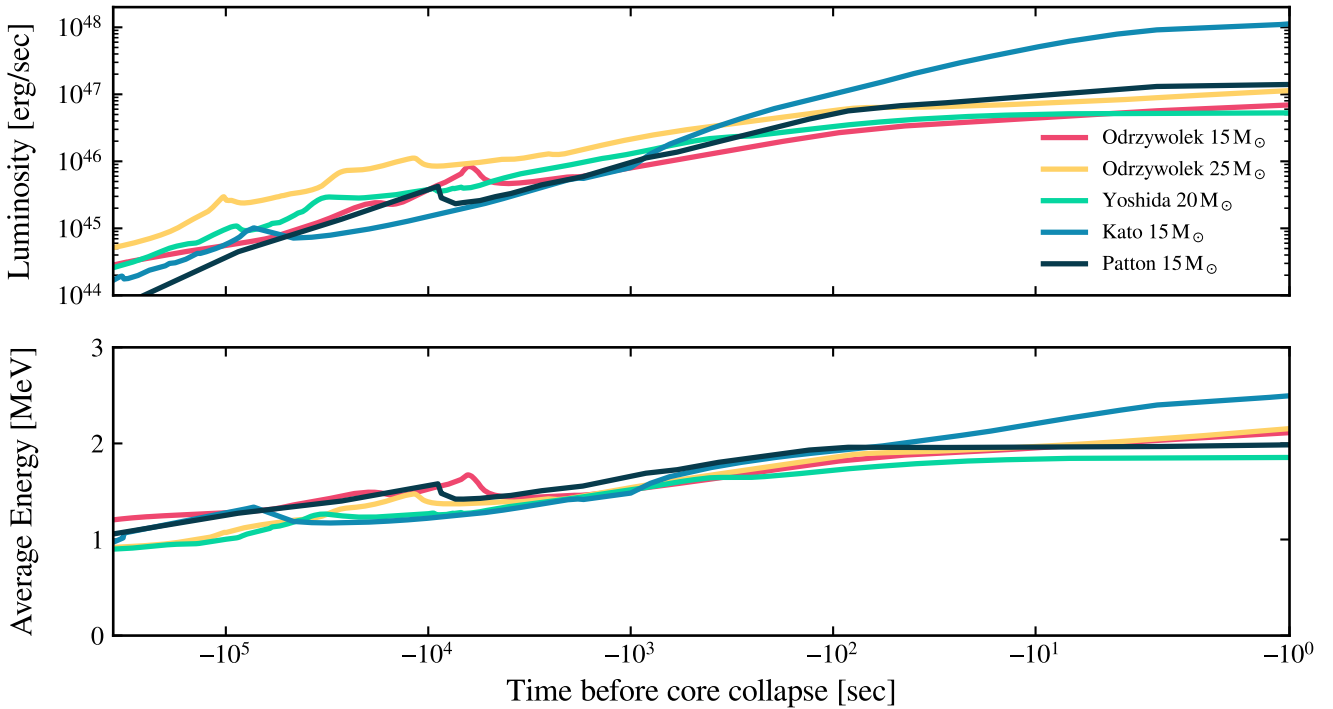
The Odrzywolek model (A. Odrzywolek et al. (2004), A. Odrzywolek & A. Heger (2010)) provides the neutrino flux which comes from thermal pair production. The production rate is based on the temperature, density and electron fraction under the nuclear statistical equilibrium as obtained from stellar-evolution calculations (S. E. Woosley et al. (2002)). Since that implementation explicitly provides only the electron-(anti)neutrino component, the non-electron-(anti)neutrino flux is assumed to be 0.19 times that of the electron-(anti)neutrinos. The Yoshida (T. Yoshida et al. (2016)) and Kato models (C. Kato et al. (2017)) use the same stellar evolution code calculated by K. Takahashi et al. (2013) and K. Takahashi et al. (2016), but differ in their treatment of microphysics. The Yoshida model considers only thermal pair production. In contrast, the Kato model performs a more comprehensive calculation that includes nuclear weak interactions, such as beta decay and electron/positron captures for 3928 nuclei calculated via post-processing (C. Kato et al. (2020)), in addition to thermal processes. Similarly, the Patton model (K. M. Patton et al. (2017)) incorporates both thermal pair production and nuclear weak interactions. This model evaluates the neutrino energy spectra using the stellar evolution code MESA (Modules for Experiments in Stellar Astrophysics), which couples the hydrodynamics with a 204-isotope nuclear network (B. Paxton et al. (2011)). Table 1 summarizes these pre-SN models. Figure 1 shows the corresponding simulated light curves and energy spectra. The exhaustion of nuclear fuel leads to core contraction, which ignites the surrounding shell. At the onset of each new shell burning phase, core expansion temporarily reduces the central temperature and density (C. Kato et al. (2020)). This decrease leads to a suppression of the neutrino emission from the core. The peaks and dips of the light curve and energy in Figure 1 are associated with the oxygen- and the silicon-shell burning.

Pre-SN $\bar{\nu}_e$ undergo flavor conversion via the Mikheyev-Smirnov-Wolfenstein (MSW) effect in the high-density environment of the stellar envelope. This flavor conversion occurs because the flavor and mass eigenstates differ in matter, and the resonance conditions in the MSW effect enhance the transition probabilities. As a result, a portion of the original $\bar{\nu}_e$ flux converts into the other flavor neutrinos, and vice versa. The observable $\bar{\nu}_e$ flux ($F_{\bar{\nu}_e}$) is

⁷ The web page of combined pre-SN alarm system between KamLAND and SK: <https://www.lowbg.org/presnalarm/>

Table 1. Representative pre-SN light curve models

| Model name | Stellar evolution code | Included reaction channels |
|-------------------|--------------------------------|-------------------------------------|
| Odrzywolek (2010) | Woosley et al. (2002) | Pair production |
| Yoshida (2016) | Takahashi et al. (2013 & 2016) | Pair production |
| Kato (2017) | Takahashi et al. (2013 & 2016) | Pair production+nuclear interaction |
| Patton (2017) | MESA | Pair production+nuclear interaction |

**Figure 1.** Electron antineutrino luminosity and their average energy are shown as a function of time before core collapse (horizontal axis). Oxygen- and Silicon-shell burning produce peaks around -10^5 s and -10^4 s before core collapse, respectively.

The pre-SN neutrino light curve models are summarized in Table 1.

$F_{\bar{\nu}_e} = pF_{\bar{\nu}_e}^0 + (1-p)F_{\bar{\nu}_x}^0$, where $F_{\bar{\nu}_e}^0$ ($F_{\bar{\nu}_x}^0$) denotes the original (non)-electron antineutrino flux. The survival probability is $p = \cos^2 \theta_{12} \cos^2 \theta_{13} = 0.680$ for the normal neutrino mass ordering (NO) and $p = \sin^2 \theta_{13} = 0.023$ for the inverted neutrino mass ordering (IO) (A. Gando et al. (2013)).

3. DETECTOR

3.1. *KamLAND*

The Kamioka Liquid scintillator Anti-Neutrino Detector (KamLAND) is located 1,000 m beneath Mt. Ikenoyama (36.42°N, 137.31°E) in Japan. KamLAND comprises 1 kt of purified organic liquid scintillator (KamLS), contained within a 13-m-diameter spherical balloon made of the 135-μm-thick nylon/EVOH film. Scintillation light is collected by the array of 1325 17-inch and 554 20-inch photomultiplier tubes (PMTs), facing the detector center. The event vertex is reconstructed using hit-time and charge information from the 17-inch PMTs, while energies are reconstructed using the combined information from the 17- and 20-inch PMTs.

KamLAND detects pre-SN $\bar{\nu}_e$ via IBD interaction with a 1.806 MeV threshold. The prompt scintillation light is produced by positron and its annihilation γ s. The electron antineutrino energy $E_{\bar{\nu}_e}$ is determined by the prompt energy (E_{prompt}) including positron kinetic and annihilation energies ($2 \times 511 \text{ keV}$): $E_{\bar{\nu}_e} \simeq E_{\text{prompt}} + \bar{E}_n + 0.8 \text{ MeV}$, where \bar{E}_n is the average recoil energy ($\sim \mathcal{O}(10) \text{ keV}$). The thermal neutrons are captured with a mean lifetime of $207.5 \pm 2.8 \mu\text{s}$ on protons ($2.2 \text{ MeV } \gamma$) or carbon-12 nuclei ($4.9 \text{ MeV } \gamma$), with relative fractions of $\sim 99\%$ and $\sim 1\%$, respectively. The sub-MeV energy threshold of KamLAND is essential to explore delayed coincidence signatures, between prompt positron signal and delayed thermal neutron capture signals, thereby achieving highly effective background rejection.

For the neutrinoless double-beta decay search (KamLAND-Zen), a mini-balloon containing xenon-loaded liquid scintillator was installed in two phases: a 3.08-m-diameter balloon (2011–2015; KamLAND-Zen 400; [A. Gando et al. \(2012\)](#)) and a 3.80-m-diameter balloon (2019–2024; KamLAND-Zen 800; [S. Abe et al. \(2025\)](#)). In the next phase, a new mini-balloon is planned for KamLAND2-Zen ([S. Abe et al. \(2025\)](#)). We assume the mini-balloon will remain in place in future operation and therefore impose a mini-balloon cut on delayed events to remove backgrounds from the balloon and its support materials.

IBD candidates are selected using spatial correlation (ΔR), time difference (ΔT) between prompt and delayed signals, prompt energy (E_{prompt}) and delayed energy (E_{delayed}). The criteria are $0.9 \text{ MeV} < E_{\text{prompt}} < 4.0 \text{ MeV}$, $1.8 \text{ MeV} < E_{\text{delayed}} < 2.6 \text{ MeV}$ or $4.4 \text{ MeV} < E_{\text{delayed}} < 5.6 \text{ MeV}$, $\Delta R < 200 \text{ cm}$ and $0.5 \mu\text{s} < \Delta T < 1,000 \mu\text{s}$. A fiducial volume cut is applied to exclude regions $> 600 \text{ cm}$ from the center of the detector in order to remove the accidental coincidences that increase near the outer balloon surface ($R = 650 \text{ cm}$). The delayed events, reconstructed within the mini-balloon, are also cut. Additionally, a likelihood cut is applied to suppress accidental coincidences.

3.2. Super-Kamiokande

Super-Kamiokande (SK) is a water-Cherenkov detector, located, like KamLAND, $\sim 1,000 \text{ m}$ underground beneath Mt. Ikenoyama. It consists of a cylindrical stainless steel tank, 39.3 m in diameter and 41.4 m in height, originally filled with 50 kt of water ([Y. Fukuda et al. \(2003\)](#)). The main detector is an inner cylinder 33.8 m in diameter and 36.2 m in height, containing approximately 32 kt of water. The standard fiducial volume of 22.5 kt is defined as the region more than 2.0 m away from the walls of the inner detector. Approximately 11,000 inward-facing 20-inch PMTs detect water Cherenkov light from neutrino interactions in the water.

In July 2020, SK began a new phase, SK-Gd, after dissolving gadolinium sulfate octahydrate ($\text{Gd}_2(\text{SO}_4)_3 \cdot 8\text{H}_2\text{O}$) to the water in the detector. Gadolinium's very large thermal-neutron capture cross section ($\sim 49,000$ barns, versus ~ 0.3 barns for hydrogen) yields an $\sim 8 \text{ MeV } \gamma$ cascade compared to a single 2.2 MeV γ from capture on hydrogen, enabling efficient neutron identification. Two loading campaigns increased the Gd concentration to 0.01% (July–August 2020; [K. Abe et al. \(2022\)](#)) and to 0.03% (May–July 2022; [K. Abe et al. \(2024\)](#)), enhancing the thermal neutron capture efficiency to $\simeq 75\%$.

With enhanced thermal neutron capture rate on Gd, SK can search for pre-SN $\bar{\nu}_e$ via IBD using a delayed coincidence between the prompt positron and delayed neutron capture, requiring $\Delta R < 300 \text{ cm}$ and $\Delta T < 80 \mu\text{s}$. IBD event selection is based on two different levels of boosted decision tree (BDT): the pre-selection $\text{BDT}_{\text{online}}$ and the final selection $\text{BDT}_{\text{offline}}$, balancing between the computational speed and the classification performance ([L. N. Machado et al. \(2022\)](#)).

4. BACKGROUND

Pre-SN neutrino searches face several background sources: electron antineutrinos from nuclear reactors, antineutrinos from radioactive decays within the Earth (geoneutrinos), and non-neutrino processes such as (α, n) reactions and accidental coincidences.

Reactor $\bar{\nu}_e$ events, which are one of the dominant backgrounds in this study, are produced from the beta decay of the fission products of neutron-rich ^{235}U , ^{238}U , ^{239}Pu and ^{241}Pu nuclides in reactors operating in Japan and Korea. The beta spectrum of each nucleus follows [P. Huber \(2011\)](#), [T. A. Mueller et al. \(2011\)](#) and [P. Vogel et al. \(1981\)](#). Although all Japanese reactors were shut down after the 2011 Great East Japan Earthquake under strengthened safety regulations, several units have gradually resumed operation since 2015. We calculate reactor $\bar{\nu}_e$ event rate, by weighting each core with its reported real-time electric (thermal) power output. The $\bar{\nu}_e$ survival probability is computed with these parameters: $\Delta m_{21}^2 = 7.53 \times 10^{-5} \text{ eV}^2$, $\tan^2 \theta_{12} = 0.436$ and $\sin^2 \theta_{13} = 0.023$ ([A. Gando et al. \(2013\)](#)). Geoneutrino events, produced in decay chains of ^{238}U and ^{232}Th nuclei inside Earth, also contribute as an additional background. The expected geoneutrino event rate is calculated using the parameters from [S. Enomoto et al. \(2007\)](#).

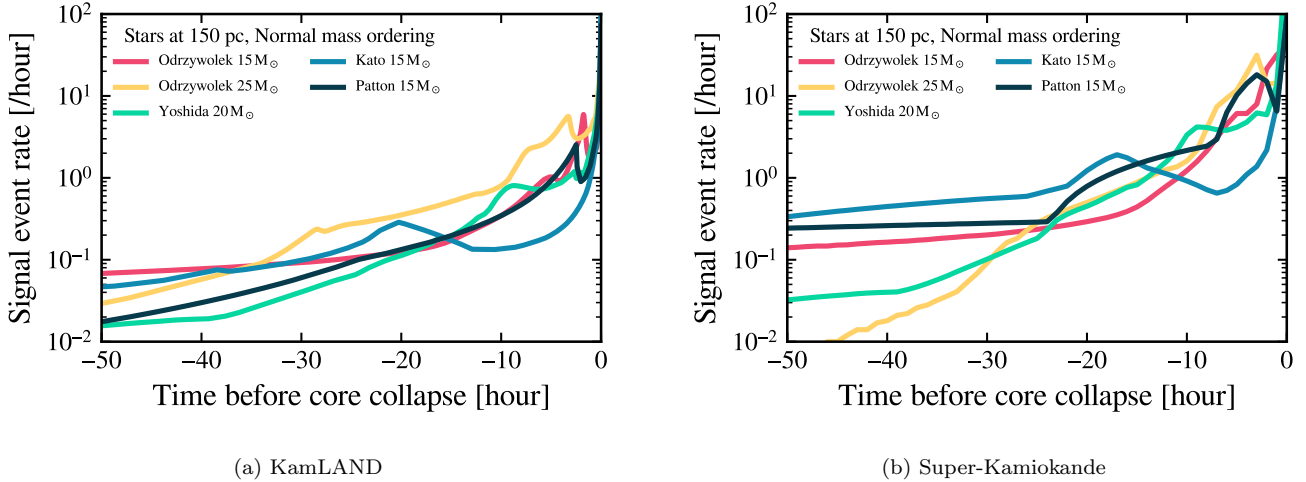


Figure 2. Time evolution of pre-SN event rate in (a) KamLAND and (b) Super-Kamiokande for the stars at 150 pc. The mass orderings are assumed to be normal. The pre-SN neutrino light curve models are summarized in Table 1.

(α, n) reactions originate from α emitters in detector materials and can yield two correlated signals that satisfy the IBD selection. In particular, $^{13}\text{C}(\alpha, n)^{16}\text{O}$ in KamLAND (S. Abe et al. (2008)), $^{18}\text{O}(\alpha, n)^{21}\text{Ne}^*$ and $^{17}\text{O}(\alpha, n)^{20}\text{Ne}^*$ in SK constitute non-negligible backgrounds. Although accidental coincidences are strongly suppressed, the residual events constitute a part of the main backgrounds.

Background rates for KamLAND and SK-Gd are taken from S. Abe et al. (2024) under the “medium reactor-activity” scenario representative of 2024 operations, which assumes full-power running of nearby Japanese reactors (Mihamata-3; Ohi-3,4; Takahama-1–4) and relevant Korean reactors. The total background rates are 0.19 day^{-1} in KamLAND and 12.4 day^{-1} in SK.

5. CONVENTIONAL ALARM METHOD

As described in the previous section, KamLAND and SK detect pre-SN $\bar{\nu}_e$ via IBD and the expected IBD event rates are calculated from the $\bar{\nu}_e$ luminosity and energy spectrum. The resulting time evolutions for both detectors are illustrated in Figure 2. Both KamLAND and SK early warning systems, for pre-SN neutrino searches, issue alarms based on the statistical significance of the excess in the observed event counts, evaluated in sliding time windows, relative to the expected background (rate analysis). The analysis time window is optimized to 24 h for KamLAND and 12 h for SK. The alarm performance characterizations are reported in (K. Asakura et al. (2016), L. N. Machado et al. (2022) and S. Abe et al. (2024)).

KamLAND enables early warning due to its lower background, whereas SK’s larger target mass allows for a rapid increase in significance and sensitivity to distant stars. By leveraging these complementary advantages and compensating for each other’s dead time, the combined alarm system achieves earlier alert times than individual detectors. It likewise employs a rate-based analysis of the event counts in the two detectors and has operated since 2023 (S. Abe et al. (2024)). Combined alarm system issues an alarm earlier than individual detectors (S. Abe et al. (2024)).

6. ALARM METHODOLOGY

Using the neutrino light curve, a new alarm method (rate+time analysis) is proposed, formulated as a one-sided hypothesis test between background-only H_0 and signal+background H_1 . The resulting p-value quantifies the significance against H_0 . In the rate+time analysis, let the data within a sliding analysis window $[t_0 - T, t_0]$ be the event count n and the set of timestamps $\{t_i\}_{i=1,2,\dots,n}$, where t_0 denotes the observation time (the end of the analysis window).

The expected pre-SN signal rate is a function of time relative to the core collapse, $R_s(t - t^*)$, where t^* is the start time of core collapse. The background rate is $R_B(t)$. The expected signal event count $S(t^*)$ and background count B over the time window T (from $t_0 - T$) are the integrals of these rates:

$$S(t^*) = \int_{t_0 - T}^{t_0} R_s(t - t^*) dt \quad \text{and} \quad B = \int_{t_0 - T}^{t_0} R_B(t) dt. \quad (1)$$

Under the inhomogeneous-Poisson model, the likelihood functions factorize into a Poisson term for n :

$$\mathcal{L}_{\text{BG+Signal}}(n, \{t_i\}, t_*) = \frac{(S(t_*) + B)^n}{n!} e^{-[S(t_*) + B]} \times \prod_{i=1}^n \frac{1}{S(t_*) + B} [R_S(t_i - t_*) + R_B(t_i)], \quad (2)$$

$$\mathcal{L}_{\text{BG Only}}(n) = \frac{B^n}{n!} e^{-B} \times \prod_{i=1}^n \frac{R_B(t_i)}{B}. \quad (3)$$

In order to discriminate background-only and background+signal hypothesis efficiently, we use log likelihood ratio function (LLR),

$$\text{LLR}(n, \{t_i\}, t_*) = \log \frac{\mathcal{L}_{\text{BG+Signal}}(n, \{t_i\}, t_*)}{\mathcal{L}_{\text{BG Only}}(n, \{t_i\})}. \quad (4)$$

The LLR is profiled over the nuisance parameter t_* to define the test statistic:

$$\Lambda(n, \{t_i\}) = \max_{t_*} \text{LLR}(n, \{t_i\}, t_*). \quad (5)$$

For the combined alarm, the joint log-likelihood ratio is given by the sum of the individual log-likelihood ratios, assuming independent data streams, and is profiled over a common t_* .

The online alarm system continuously calculates Λ in sliding window. The alarm system introduces a trials factor (look-elsewhere effect) that would otherwise inflate naive significances. We therefore calibrate the global p-value and the false alarm rate (FAR) using toy Monte Carlo under H_0 (background-only), measuring how often Λ exceeds a threshold in continuous operation. This statistical test depends on a reference pre-SN neutrino light-curve model. In this study, we evaluate an ensemble of models and report the minimum FAR across the model set.

7. ALARM SENSITIVITY TO PRE-SUPERNOVA NEUTRINOS

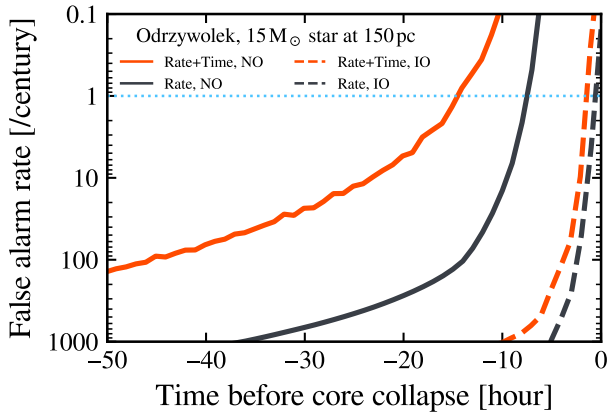
The performance of the proposed method is evaluated for KamLAND, SK and their combined sensitivity. Signal injections are generated from the models by Odrzywolek and Patton, assuming a $15 M_\odot$ star at 150 pc with either normal or inverted neutrino mass ordering, following [S. Abe et al. \(2024\)](#). The reference light-curve models used in the likelihood are those listed in Table 1. We focus on the alarm performance for α Orionis (Betelgeuse), a nearby candidate for a future core collapse event. Observational studies suggest that Betelgeuse has an initial mass in the range $17\text{--}25 M_\odot$ ([M. M. Dolan et al. \(2016\)](#), [M. Joyce et al. \(2020\)](#)). Conservatively, we adopt $15\text{--}25 M_\odot$ for the reference. To assess robustness to model mismatch, we evaluate sensitivity when the injected true pre-SN light curve model differs from the reference model; unless otherwise noted, the reference assumes a star at 150 pc with normal neutrino mass ordering, because it predicts a higher survival probability than inverted neutrino mass ordering, resulting in a larger observable event rate while retaining similar temporal features.

Figure 3 compares the time evolution of the expected FAR between rate-only and rate+time analysis for KamLAND. The analysis time window for the rate+time analysis is set to 200 h, roughly spanning from the onset of silicon burning to core collapse. The horizontal dashed line marks a FAR of one per century. For an injection based on the Odrzywolek model with normal neutrino mass ordering, the KamLAND rate+time method achieves the best performance among the tested configurations and issues an alert ≥ 14.5 h before core collapse. Figure 4 shows the SK FAR comparison. The analysis time window for the SK rate+time analysis is set to 48 h. In the most favorable case, the SK rate+time analysis issues an alert ≥ 11.6 h before core collapse.

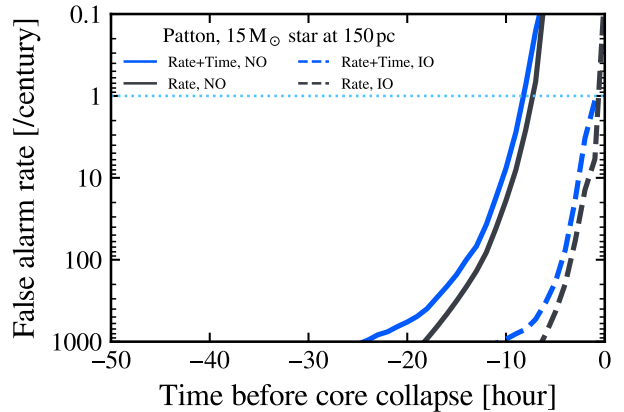
For the combined KamLAND and SK alarm, sensitivities are evaluated with independent time-series Monte Carlo for each detector. The resulting FAR is shown in Figure 5. The combined rate+time analysis improves sensitivity and delivers earlier alerts than either detector alone.

8. DISCUSSION

Table 2 summarizes the alarm lead times (hours before core collapse) for KamLAND, SK, and their combined configuration. For each individual detector, the rate+time analysis achieves lead times comparable to those of the combined rate-only analysis. Even if one detector is inoperative, the other maintains performance comparable to the conventional combined (rate-only) system. Furthermore, the combined rate+time analysis yields the earliest alerts among all configurations: For a $15 M_\odot$ star at 150 pc, assuming normal neutrino mass ordering, it provides a warning

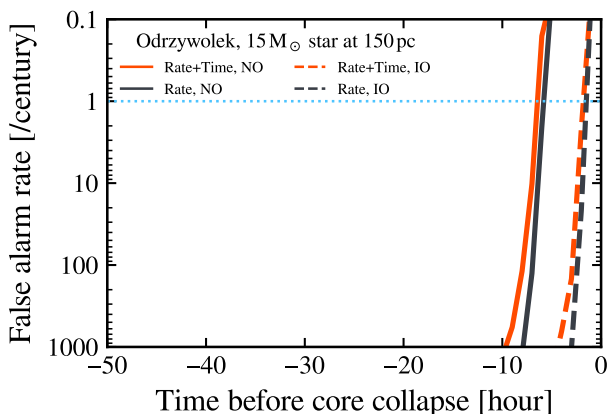


(a) Odrzywolek model signal

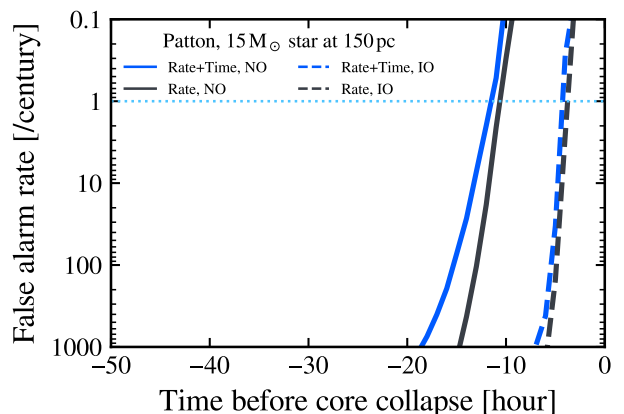


(b) Patton model signal

Figure 3. Time evolution of expected FAR in KamLAND. (a) presents the alarm sensitivity of Odrzywolek model. (b) presents the alarm sensitivity of Patton model. The horizontal dashed light-blue line represents FAR of 1/century.



(a) Odrzywolek model signal



(b) Patton model signal

Figure 4. Time evolution of expected FAR in SK. (a) presents the alarm sensitivity of Odrzywolek model. (b) presents the alarm sensitivity of Patton model. The horizontal dashed light-blue line represents FAR of 1/century.

14.0 h (Odrzywolek model) and 14.7 h (Patton model) before core collapse whereas rate analysis yields 8.2 h and 12.3 h respectively.

Beyond earlier alerts, the rate+time analysis enhances sensitivity to more distant sources relative to rate-only methods. Since the pre-SN neutrino signal decreases with the square of the distance, leveraging temporal information allows statistically significant alerts with fewer events, enabling detection of weaker signals that may be inaccessible to rate-only analyses.

9. SUMMARY

We introduced an early-warning method based on the time evolution of the pre-SN neutrino event rate (“rate+time” analysis). The alarm method uses multiple time profiles, derived from representative pre-SN neutrino light curve models A. Odrzywolek et al. (2004), A. Odrzywolek & A. Heger (2010), T. Yoshida et al. (2016), C. Kato et al. (2017) and K. M. Patton et al. (2017) in the mass range of $15\text{--}25 M_{\odot}$, to ensure robustness. Background rates are calculated assuming full-power operation of Japanese commercial reactors near the Kamioka mine (Mihamata-3; Ohi-3,4; Takahama-1–4) and relevant Korean reactors.

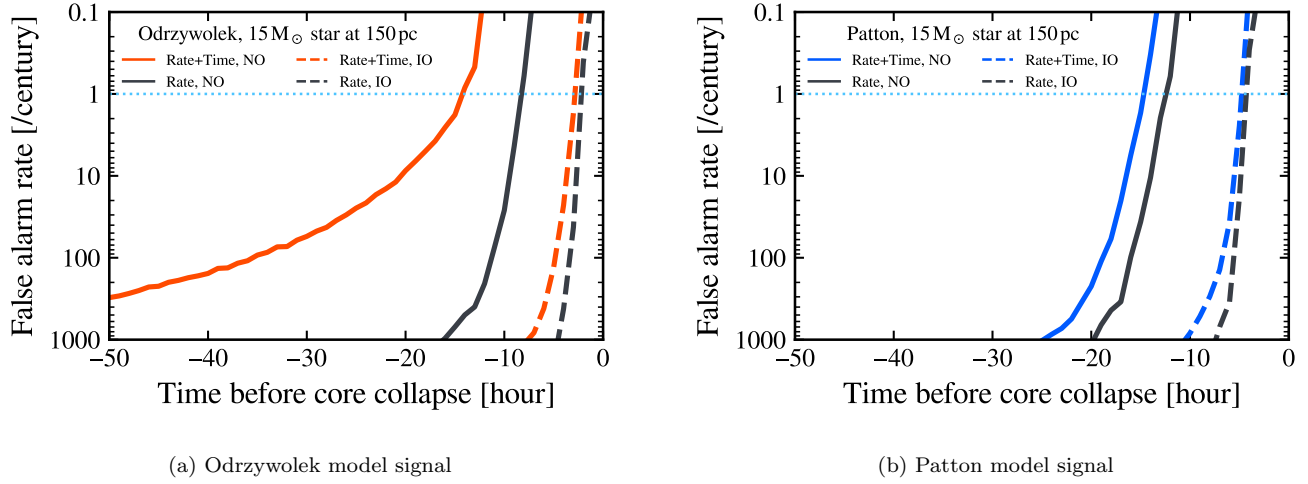


Figure 5. Time evolution of expected FAR in combined alarm case. (a) presents the alarm sensitivity of Odrzywolek model. (b) presents the alarm sensitivity of Patton model. The horizontal dashed light-blue line represents FAR of 1 /century.

Table 2. Warning times [hours] before core collapse of $15 M_{\odot}$ stars at 150 pc. The alarm threshold is FAR of 1 /century.

| Detector | Analysis | Warning time [hour] | | | |
|----------|-----------|---------------------------|-----|-----------------------|-----|
| | | Odrzywolek $15 M_{\odot}$ | | Patton $15 M_{\odot}$ | |
| | | NO | IO | NO | IO |
| KamLAND | Rate | 7.5 | N/A | 7.3 | 0.2 |
| | Rate+time | 14.5 | 1.6 | 8.2 | 0.9 |
| SK | Rate | 5.8 | 1.6 | 10.5 | 3.8 |
| | Rate+time | 6.3 | 1.9 | 11.6 | 4.3 |
| Combined | Rate | 8.2 | 2.1 | 12.3 | 4.3 |
| | Rate+time | 14.0 | 2.8 | 14.7 | 4.8 |

We also evaluated the alarm sensitivity of rate+time analysis for a $15 M_{\odot}$ star at 150 pc in KamLAND, SK and their combined configuration. The analysis time window of rate+time analysis is 200 h in KamLAND and 48 h in SK. The rate+time analysis issues earlier alarms than the conventional rate-only method. The optimistic alarm time is 14.5 h and 11.6 h before core collapse in KamLAND and SK, respectively. Using the combined system with the rate+time analysis yields the earliest alerts overall, up to 14.7 h in the optimistic case, compared to 12.3 h for the combined rate-only analysis.

ACKNOWLEDGEMENTS

This work is supported by JSPS KAKENHI Grant Numbers 24H02237, 24H02242, 25KJ0557, and 24H00243, the Science and Technology Facilities Council (STFC). We would like to thank all KamLAND and Super-Kamiokande collaborators for supporting this effort.

REFERENCES

- Abe, K., Abe, K., Aihara, H., et al. 2018, arXiv e-prints, arXiv:1805.04163, doi: [10.48550/arXiv.1805.04163](https://doi.org/10.48550/arXiv.1805.04163)
- Abe, K., et al. 2022, Nucl. Instrum. Meth. A, 1027, 166248, doi: [10.1016/j.nima.2021.166248](https://doi.org/10.1016/j.nima.2021.166248)
- Abe, K., Bronner, C., Hayato, Y., et al. 2024, Nuclear Instruments and Methods in Physics Research A, 1065, 169480, doi: [10.1016/j.nima.2024.169480](https://doi.org/10.1016/j.nima.2024.169480)
- Abe, S., et al. 2008, Phys. Rev. Lett., 100, 221803, doi: [10.1103/PhysRevLett.100.221803](https://doi.org/10.1103/PhysRevLett.100.221803)
- Abe, S., et al. 2024, Astrophys. J., 973, 140, doi: [10.3847/1538-4357/ad5fee](https://doi.org/10.3847/1538-4357/ad5fee)
- Abe, S., Araki, T., Chiba, K., et al. 2025, Phys. Rev. Lett., 135, 262501, doi: [10.1103/jkfl6-48j8](https://doi.org/10.1103/jkfl6-48j8)
- Abi, B., et al. 2021, Eur. Phys. J. C, 81, 423, doi: [10.1140/epjc/s10052-021-09166-w](https://doi.org/10.1140/epjc/s10052-021-09166-w)
- Abusleme, A., Adam, T., Ahmad, S., et al. 2024, JCAP, 2024, 057, doi: [10.1088/1475-7516/2024/01/057](https://doi.org/10.1088/1475-7516/2024/01/057)
- Al Kharusi, S., BenZvi, S. Y., Bobowski, J. S., et al. 2021, New Journal of Physics, 23, 031201, doi: [10.1088/1367-2630/abde33](https://doi.org/10.1088/1367-2630/abde33)
- Albanese, V., Alves, R., Anderson, M. R., et al. 2021, arXiv e-prints, arXiv:2104.11687, doi: [10.48550/arXiv.2104.11687](https://doi.org/10.48550/arXiv.2104.11687)
- Alekseev, E. N., Alekseeva, L. N., Volchenko, V. I., & Krivosheina, I. V. 1987, JETP Lett., 45, 589
- Antonioli, P., et al. 2004, New J. Phys., 6, 114, doi: [10.1088/1367-2630/6/1/114](https://doi.org/10.1088/1367-2630/6/1/114)
- Asakura, K., et al. 2016, Astrophys. J., 818, 91, doi: [10.3847/0004-637X/818/1/91](https://doi.org/10.3847/0004-637X/818/1/91)
- Bionta, R. M., et al. 1987, Phys. Rev. Lett., 58, 1494, doi: [10.1103/PhysRevLett.58.1494](https://doi.org/10.1103/PhysRevLett.58.1494)
- Dolan, M. M., Mathews, G. J., Lam, D. D., et al. 2016, ApJ, 819, 7, doi: [10.3847/0004-637X/819/1/7](https://doi.org/10.3847/0004-637X/819/1/7)
- Enomoto, S., Ohtani, E., Inoue, K., & Suzuki, A. 2007, Earth and Planetary Science Letters, 258, 147, doi: <https://doi.org/10.1016/j.epsl.2007.03.038>
- Fukuda, Y., et al. 2003, Nucl. Instrum. Meth. A, 501, 418, doi: [10.1016/S0168-9002\(03\)00425-X](https://doi.org/10.1016/S0168-9002(03)00425-X)
- Gando, A., et al. 2012, Phys. Rev. C, 85, 045504, doi: [10.1103/PhysRevC.85.045504](https://doi.org/10.1103/PhysRevC.85.045504)
- Gando, A., et al. 2013, Phys. Rev. D, 88, 033001, doi: [10.1103/PhysRevD.88.033001](https://doi.org/10.1103/PhysRevD.88.033001)
- Hirata, K., et al. 1987, Phys. Rev. Lett., 58, 1490, doi: [10.1103/PhysRevLett.58.1490](https://doi.org/10.1103/PhysRevLett.58.1490)
- Huber, P. 2011, Phys. Rev. C, 84, 024617, doi: [10.1103/PhysRevC.84.024617](https://doi.org/10.1103/PhysRevC.84.024617)
- Joyce, M., Leung, S.-C., Molnár, L., et al. 2020, The Astrophysical Journal, 902, 63, doi: [10.3847/1538-4357/abb8db](https://doi.org/10.3847/1538-4357/abb8db)
- Kato, C., Delfan Azari, M., Yamada, S., et al. 2015, ApJ, 808, 168, doi: [10.1088/0004-637X/808/2/168](https://doi.org/10.1088/0004-637X/808/2/168)
- Kato, C., Ishidoshiro, K., & Yoshida, T. 2020, Annual Review of Nuclear and Particle Science, 70, 121, doi: [10.1146/annurev-nucl-040620-021320](https://doi.org/10.1146/annurev-nucl-040620-021320)
- Kato, C., Nagakura, H., Furusawa, S., et al. 2017, Astrophys. J., 848, 48, doi: [10.3847/1538-4357/aa8b72](https://doi.org/10.3847/1538-4357/aa8b72)
- Machado, L. N., et al. 2022, Astrophys. J., 935, 40, doi: [10.3847/1538-4357/ac7f9c](https://doi.org/10.3847/1538-4357/ac7f9c)
- Mueller, T. A., Lhuillier, D., Fallot, M., et al. 2011, Phys. Rev. C, 83, 054615, doi: [10.1103/PhysRevC.83.054615](https://doi.org/10.1103/PhysRevC.83.054615)
- Odrzywolek, A., & Heger, A. 2010, Acta Phys. Polon. B, 41, 1611
- Odrzywolek, A., Misiaszek, M., & Kutschera, M. 2004, Astropart. Phys., 21, 303, doi: [10.1016/j.astropartphys.2004.02.002](https://doi.org/10.1016/j.astropartphys.2004.02.002)
- Pagliaroli, G., Vissani, F., Costantini, M. L., & Ianni, A. 2009, Astroparticle Physics, 31, 163, doi: [10.1016/j.astropartphys.2008.12.010](https://doi.org/10.1016/j.astropartphys.2008.12.010)
- Patton, K. M., Lunardini, C., Farmer, R. J., & Timmes, F. X. 2017, Astrophys. J., 851, 6, doi: [10.3847/1538-4357/aa95c4](https://doi.org/10.3847/1538-4357/aa95c4)
- Paxton, B., Bildsten, L., Dotter, A., et al. 2011, Astrophys. J. Suppl., 192, 3, doi: [10.1088/0067-0049/192/1/3](https://doi.org/10.1088/0067-0049/192/1/3)
- Pietrzyński, G., Graczyk, D., Galleenne, A., et al. 2019, Nature, 567, 200, doi: [10.1038/s41586-019-0999-4](https://doi.org/10.1038/s41586-019-0999-4)
- Raj, N., Takhistov, V., & Witte, S. J. 2020, Phys. Rev. D, 101, 043008, doi: [10.1103/PhysRevD.101.043008](https://doi.org/10.1103/PhysRevD.101.043008)
- Scholberg, K. 2012, Annual Review of Nuclear and Particle Science, 62, 81, doi: [10.1146/annurev-nucl-102711-095006](https://doi.org/10.1146/annurev-nucl-102711-095006)
- Sheshukov, A., Vishneva, A., & Habig, A. 2021, JCAP, 2021, 053, doi: [10.1088/1475-7516/2021/12/053](https://doi.org/10.1088/1475-7516/2021/12/053)
- Suzuki, A. 2014, Eur. Phys. J. C, 74, 3094, doi: [10.1140/epjc/s10052-014-3094-x](https://doi.org/10.1140/epjc/s10052-014-3094-x)
- Takahashi, K., Yoshida, T., & Umeda, H. 2013, ApJ, 771, 28, doi: [10.1088/0004-637X/771/1/28](https://doi.org/10.1088/0004-637X/771/1/28)
- Takahashi, K., Yoshida, T., Umeda, H., Sumiyoshi, K., & Yamada, S. 2016, MNRAS, 456, 1320, doi: [10.1093/mnras/stv2649](https://doi.org/10.1093/mnras/stv2649)
- Vogel, P., Schenter, G. K., Mann, F. M., & Schenter, R. E. 1981, Phys. Rev. C, 24, 1543, doi: [10.1103/PhysRevC.24.1543](https://doi.org/10.1103/PhysRevC.24.1543)
- Woosley, S. E., Heger, A., & Weaver, T. A. 2002, Rev. Mod. Phys., 74, 1015, doi: [10.1103/RevModPhys.74.1015](https://doi.org/10.1103/RevModPhys.74.1015)
- Yoshida, T., Takahashi, K., Umeda, H., & Ishidoshiro, K. 2016, PhRvD, 93, 123012, doi: [10.1103/PhysRevD.93.123012](https://doi.org/10.1103/PhysRevD.93.123012)